

## STRUCTURAL AND MAGNETIC PROPERTIES OF MgFeCrO<sub>4</sub> FERRITE NANOPARTICLES

H. MEHRANFAR<sup>a,\*</sup>, M. M. MOHAMMED<sup>b</sup>, A. M. MOHAMMAD<sup>a</sup>

<sup>a</sup>University of Garmian, College of Education, Department of Physics, Kurdistan region, Iraq

<sup>b</sup>University of Garmian, College of Education, Department of Chemistry, Kurdistan region, Iraq

In this paper, we have synthesized MgFeCrO<sub>4</sub> ferrite Nanoparticles by using sol-gel auto combustion method and calcined for 3h at 600, 700, 800 and 900 °C. Investigating the prepared ferrites, we have employed different characterization methods such as X-ray Diffraction (XRD), Field Emission Scanning Electron Microscopy (FE-SEM), Energy Dispersive Spectrum (EDS), Thermo-gravimetric analysis (TGA) and Vibrating Sample Magnetometer (VSM). The XRD patterns of the synthesized samples revealed all the major peaks corresponding to the single spinel structure and once the calcination temperature was elevated, the diffraction peaks became sharper, narrower and more intense. The nanoscale of the synthesized ferrite was identified by FE-SEM investigation and revealed some agglomerated of spherical shape morphology. EDS spectra showed peaks corresponding to the elements Mg, Fe, Cr, and O and all prepared samples exhibited the chemical composition similar to the proposed stoichiometric formula. The TGA analysis for the sample calcined at 700 °C indicated the decomposition of precursors. The crystallization of ferrite was completed at above 600 °C. The VSM results showed that the magnetic properties were centered on the calcination temperature; thus, as the calcination temperature elevated, the saturation magnetization decreased and coercivity increased. Consequently, the value of remanence magnetization increased at the calcination temperature from 700 to 800 °C and then dropped at 900 °C.

(Received June 2, 2019; Accepted July 15, 2019)

*Keywords:* Nanoparticle, Spinel ferrites, Sol-gel auto combustion, Magnetic properties

### 1. Introduction

Ferrite materials have become the subject of research interest in recent years. They have been used for innumerable applications and therefore can be considered as one of the most important materials [1]. The properties of these materials can be tuned easily due to the anion-cation bond framework that connects the tetrahedral and octahedral sublattices with the structure capable of adopting a wide variety of ions at A and B sites. The magnetic and electronic properties could be strongly affected by alteration in cation distribution among tetrahedral and octahedral sites.

Among all ferrites, cobalt ferrite has aroused intense interests because of its chemical stability and large cubic magnetic anisotropy; it is also known to be a photo-magnetic material with high coercivity [2, 3]. Furthermore, it is been reported that nanoparticles are synthesized by a number of synthetic routes such as co-precipitation, microemulsion, thermal decomposition, hydrothermal synthesis and sonochemical synthesis [4]. Sol-gel method is the most conventional method employed to synthesize metal oxides. Hydrolysis, condensation, and drying process are the steps at which the starting materials undergo the synthesis of the metal oxide. Chlorides or metal oxides are used as a precursor for the formation of colloids solution where they go through three steps [5]. In this manuscript, we investigate the magnetic properties of MgFeCrO<sub>4</sub> ferrite nanoparticles synthesized by the sol-gel auto combustion method.

## 2. Experimental details

### 2.1. Synthesis

Ferrite nanoparticles with chemical formula  $\text{MgFeCrO}_4$  were synthesized in the air using citrate-gel auto combustion method. Stoichiometric amounts of magnesium nitrate  $\text{Mg}(\text{NO}_3)_2 \cdot 6\text{H}_2\text{O}$ , ferric nitrate  $\text{Fe}(\text{NO}_3)_3 \cdot 9\text{H}_2\text{O}$ , chromium nitrate  $\text{Cr}(\text{NO}_3)_3 \cdot 9\text{H}_2\text{O}$  and citric acid  $\text{C}_6\text{H}_8\text{O}_7$  in mole ratio of (citric acid: nitrates =1:1) were weighed and dissolved separately in a minimum amount of deionized water to form a mixed solution. After stirring, the pH of solution was adjusted to 7 by adding ammonia solution dropwise [6]. The obtained solution was transformed into a viscous gel phase by slowly increasing the temperature of hot plate to  $90^\circ\text{C}$  for 2h under continuous stirring. During evaporation, the solution became a very viscous brown gel. All water molecules were removed from the mixture, the viscous gel of  $\text{MgFeCrO}_4$  was placed on an oven and heated at 275 to initiate an auto combustion reaction and produce as-burnt ferrite powder. The as-burnt powders of  $\text{MgFeCrO}_4$  nanoparticles after combustion were calcined in a programmed furnace at 600, 700, 800 and  $900^\circ\text{C}$  for 3h to remove organic waste and improve the homogeneity. Afterward, their structural and magnetic properties are set aside for further investigations.

### 2.2. Characterizations

The crystal structure of the synthesized samples was characterized using X-Ray Diffraction (XRD) and model PANalytical (X'pert Pro, Netherlands) equipped with high-intensity  $\text{Cu } \alpha$  radiation source ( $\lambda = 0.154 \text{ nm}$ , 40 mA, 40 kV) in the  $2\theta$  range ( $15^\circ$ - $80^\circ$ ). Morphology of the calcined powders at different temperature was observed by Field Emission Scanning Electron Microscopy (FE-SEM), using (FE-SEM; Model Mira3-XMU, TESCAN, Japan). Thermo-gravimetric analysis (TGA) was performed by a model TGA-STA 1500 from Rheometric Scientific (USA) under a nitrogen atmosphere at a heating rate of  $10^\circ\text{C}/\text{min}$  from ambient temperature to  $800^\circ\text{C}$ . The magnetic properties of the calcined powders have been investigated by means of Vibrating Sample Magnetometer (VSM), using an (LBKFB model Meghnatis Daghig Kavir Company) in applied field ranging from  $-15$  to  $+15 \text{ kOe}$  at room temperature.

## 3. Results and discussion

### 3.1. XRD analysis

The XRD patterns of  $\text{MgFeCrO}_4$  ferrite nanoparticles for as-burnt and the calcined powders at different temperature levels 600, 700, 800 and  $900^\circ\text{C}$  are shown in Fig. 1. It can be seen from the XRD pattern that all the reflection peaks are corresponding to (220), (311), (222), (400), (422), (511) and (440) planes. All the samples exhibit poly-oriented structure and the peak positions are in coherence with the spinel phase cubic structure (ICSD 98-011-2792).

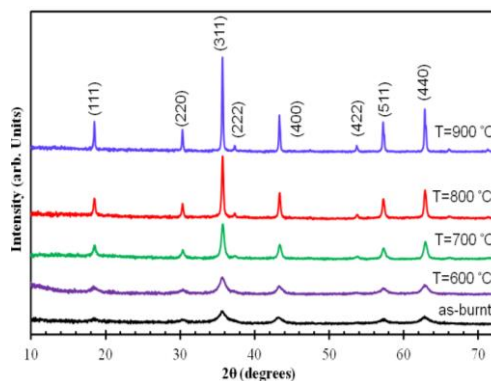


Fig. 1. XRD patterns of  $\text{MgFeCrO}_4$  nanoparticles for as-burnt and calcined at 600, 700, 800 and  $900^\circ\text{C}$ .

XRD patterns show broad peaks indicating a fine particle [7], and as the calcination temperature increases, the diffraction peaks become sharper, higher and narrower, and their intensity increases. This indicates that the intensification in crystallinity originates from the growing of crystalline volume ratio because of the particle size enlargement of the nuclei [8]; similar observation was reported by A. Mohammad et al [9]. Moreover, the non-existence of additional peaks for all compositions specifies that all the samples have pure single-phase cubic structure without any impurity peak, and the strongest reflection stems from the (311) plane among all the samples. In general, a slight shift of peak position and variety of peak widths stem from the difference in the nature of metal cations, binding energies, their ionic radius, and the site preferences. The average crystallite sizes of all samples was calculated from Scherrer's equation [10], using the peak width at half maximum intensity (FWHM) for peak (311).

$$D = \frac{K\lambda}{\beta \cos \theta} \quad (1)$$

where  $D$  is the average crystal size,  $K$  is the Scherrer coefficient (0.9),  $\lambda$  is the x-ray wavelength,  $\theta$  is Bragg's angle ( $2\theta$ ) and  $\beta$  the full width at half-maximum (FWHM) in radians. The crystallite sizes of (6.37, 8.69, 21.01, 37.07 and 54.16 nm) were obtained for as-burnt and calcined at 600, 700, 800 and 900 °C, respectively. Table 1, clearly shows that with the increase in the calcination temperature, the crystallite size increases, and the crystallite grows up from mean size of 8.69 nm at 600 °C to 21.01 nm at 700 °C. The results show that the reaction temperatures at 700 °C and above are suitable to the growth of the  $\text{MgFeCrO}_4$  crystallite. The lattice parameter 'a' is calculated according to the following equation [11], and listed in Table 1.

$$a = d_{hkl}(h^2 + k^2 + l^2)^{1/2} \quad (2)$$

where  $d_{hkl}$  is the interplanar distance of each plane and  $(hkl)$  are Miller indices. The variation in lattice parameter of the samples is shown in Table 1, which does not appear to be a simple linear function (approximately have the same value) and the lattice parameter is influenced by many factors such as the size of the atoms, interactive forces between the atoms [12], size of the final particle/grain [13] etc. The X-ray density ( $\rho_x$ ) is dependent on the molar mass of the synthesized compounds and the lattice parameter 'a' which was calculated using the relation [14]:

$$\rho_x = \frac{8M}{Na^3} \quad (3)$$

Factor 8 is the number of molecules per unit cell,  $N$  is Avogadro's number and  $M$  is the molecular weight of the sample. The values of ( $\rho_x$ ) nearly have the same value and directly correlates to the same molecular weight of all samples.

The distance between the magnetic ions known as hopping length ( $L$ ) and depended on the lattice parameter 'a', the hopping length ( $L_A$ ) in the tetrahedral A-site and ( $L_B$ ) in the octahedral B-site all can be calculated using the relations below [15]:

$$L_A = 0.25a\sqrt{3} \quad (4)$$

$$L_B = 0.25a\sqrt{2} \quad (5)$$

The calculated values of the hopping length ( $L_A$ ) and ( $L_B$ ) of all samples were listed in Table 1. It is observed that the hopping length changes slightly as the temperature changes. The changes in the calcination temperature may play an important role in the rearrangement of the cation in both tetrahedral and octahedral sites.

Table 1. Values of crystallite size ( $D$ ), Lattice parameter ' $a$ ', X-ray density ( $\rho_x$ ), hopping length ( $L_A$ ) and ( $L_B$ ) of  $MgFeCrO_4$  nanoparticles for as-burnt and calcined at 600, 700, 800 and 900 °C.

Calcinations temperature	as-burnt	600 °C	700 °C	800 °C	900 °C
$D$ (nm)	6.37	8.69	21.01	37.07	54.16
$a$ (Å)	8.36	8.36	8.35	8.36	8.35
$\rho_x$ (gm/cm <sup>3</sup> )	4.47	4.47	4.48	4.47	4.47
$L_A$ (Å)	3.6183	3.6180	3.6141	3.6180	3.6178
$L_B$ (Å)	2.9543	2.9541	2.9509	2.9541	2.9539

### 3.2. FE-SEM analysis

Micrographs of  $MgFeCrO_4$  using the field emission scanning electron microscope (FE-SEM) are shown in Fig. 2 (a-c), all samples exhibit the homogeneous grain size distribution with relatively well-crystallized grains in the nanometer range. The particles seem to be spherical and uniform in size with a tendency of agglomeration.

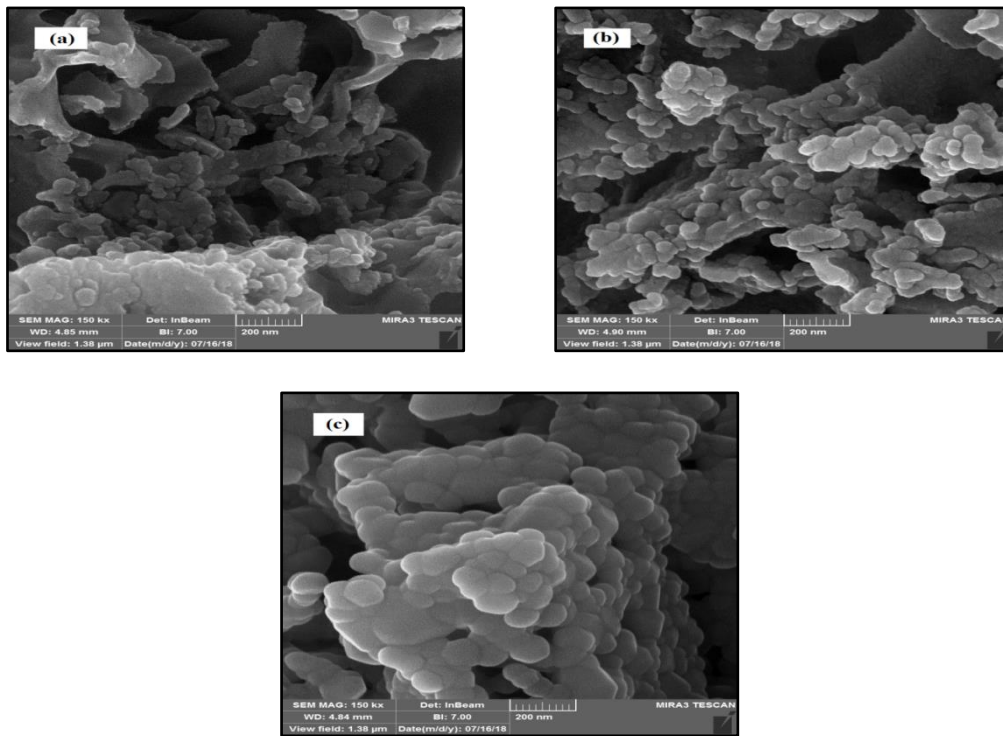


Fig. 2. FE-SEM microstructures of  $MgFeCrO_4$  nanoparticles for (a) as-burnt (b) calcined at 700 °C and (c) calcined at 900 °C.

Fig. 2 (c) shows the microstructure of the sample calcined at 900 °C along with spherical particle shapes with enhanced size. It can be seen clearly that there is an improvement among the particles compared to the samples that calcined at 275 °C (as-burnt) and 700 °C. Furthermore, micrograph revealed that the ferrite samples have few voids and porous nature agglomerates which may be attributed to the calcination process and magnetic forces or Vander Waals bonds [16, 17]. From Table 2, it can be seen that the crystallite and grain size linear increase as the calcination temperature increases. The estimated grain size is about 38.38, 45.12 and 86.02 nm for as-burnt and the samples calcined at 700 and 900 °C respectively. The agglomeration of crystallites is the main reason to observe different and little higher grain size than the crystallite size obtained using Scherrer's formula [18, 19]. In the present study, it is observed that with increasing calcination temperature the porosity was reduced.

Table 2. Average crystallite size and grain sizes of  $MgFeCrO_4$  nanoparticles for (a) as-burnt (b) calcined at  $700^\circ C$  and (c) calcined at  $900^\circ C$  determined from XRD and FE-SEM.

Calcinations temperature	as-burnt ( $300^\circ C$ )	$700^\circ C$	$900^\circ C$
$D(nm)$ XRD	6.37	21.01	54.16
$D(nm)$ FE-SEM	38.38	45.12	86.02

### 3.3. EDS spectroscopy

The EDS spectral analysis of  $MgFeCrO_4$  nanoparticles for as-burnt and the samples that calcined at  $700$  and  $900^\circ C$  are shown in Fig. 3 (a-c). The qualitative elemental analysis obtained from EDS spectra shows peaks corresponding to Mg, Fe, Cr, and O. All prepared samples exhibit chemical composition similar to the proposed stoichiometric formula and the condition of preparation completely favors the formation of mixed ferrites (random ferrite).

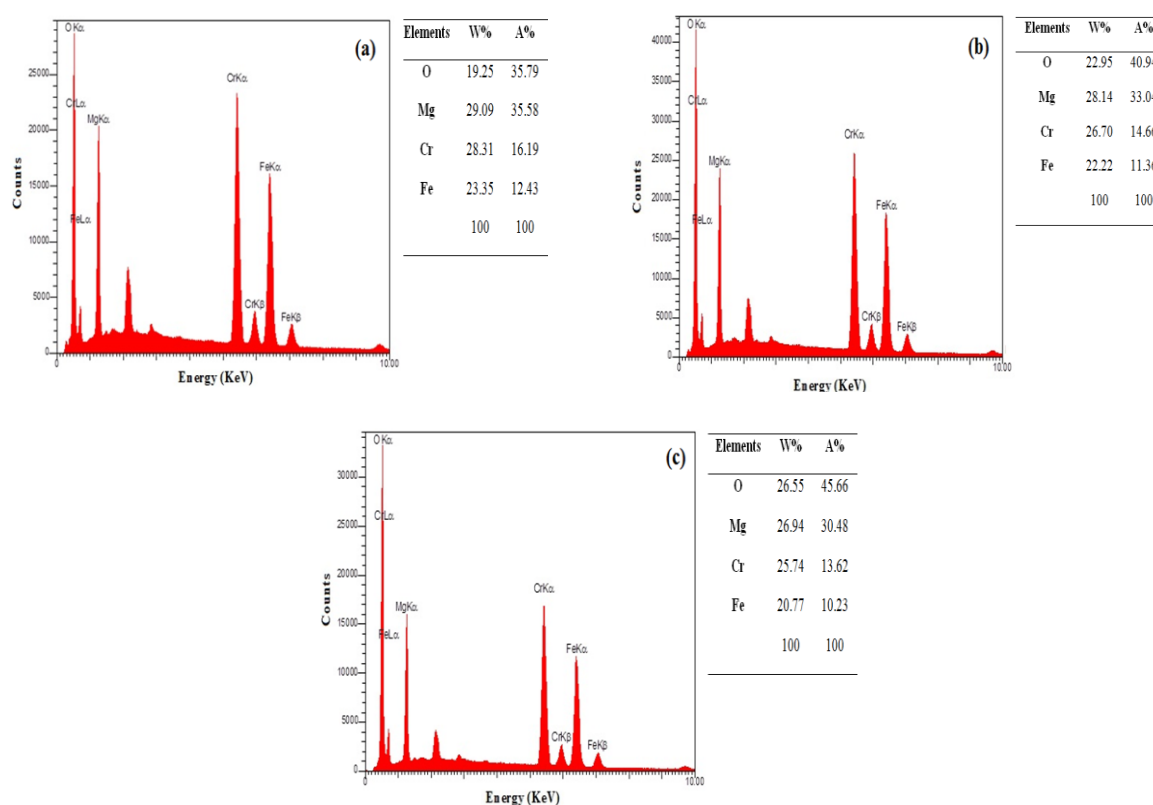


Fig. 3 EDS spectra of  $MgFeCrO_4$  nanoparticles for (a) as-burnt (b) calcined at  $700^\circ C$  and (c) calcined at  $900^\circ C$ .

### 3.4. Thermogravimetric analysis (TGA)

TGA analyses (Fig. 4) have been carried out for as-burnt and the sample calcined at  $700^\circ C$  of  $MgFeCrO_4$  nanoparticles under a nitrogen atmosphere. The as-burnt curve shows that the loss of chemically or physically absorbed of the OH groups is the main reason for weight loss below  $50^\circ C$  [20]. The loss of weight at  $350^\circ C$  is due to evaporation of absorbed water while the wet loss about  $350-600^\circ C$  is associated with residual organic matter, including citric acid; the loss of weight at below  $600^\circ C$ , however, is attributed to the loss of water absorbed and the organic derivatives decomposition [21]. The complete crystallization of the sample occurs in temperature above  $600^\circ C$ . Almost approximately no loss in weight is observed in the calcined sample at  $700^\circ C$ , which suggests the completion of decomposition of precursors and the crystallization of ferrite. This indicates the oxidation of non-reactive mineral nitrates in this step.

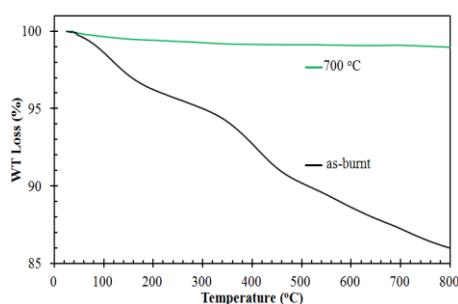


Fig. 4. TGA curves for as-burnt and calcined sample at 700 °C of MgFeCrO<sub>4</sub> nanoparticles.

### 3.5. Magnetic studies

Fig. 5 shows the hysteresis loops for the nanocrystalline MgFeCrO<sub>4</sub> nanoparticles in the sample calcined at 700, 800 and 900 °C. The hysteresis loops (M-H loop) are used for measuring the magnetic parameters such as saturation magnetization ( $M_s$ ), remanent magnetization ( $M_r$ ) and coercivity ( $H_c$ ) (Table 3). These parameters show dependence on calcination temperatures and on several factors such as porosity, density, particle size, and A–B superexchange interaction [22].

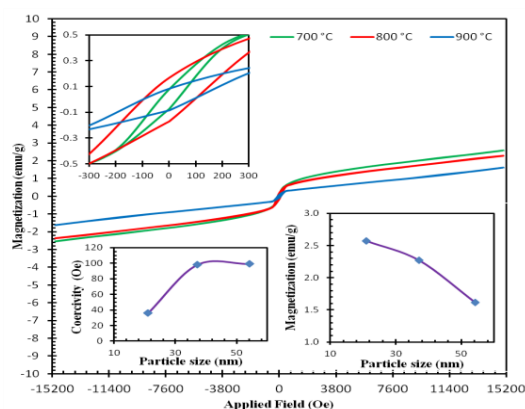


Fig. 5. Hysteresis loops of MgFeCrO<sub>4</sub> nanoparticles in the sample calcined at 700, 800 and 900 °C.

Table 3. Variation in saturation magnetization ( $M_s$ ), remanance magnetization ( $M_r$ ) and coercivity ( $H_c$ ) of MgFeCrO<sub>4</sub> nanoparticles in the sample calcined at 700, 800 and 900 °C.

Calcinations temperature	700 °C	800 °C	900 °C
$M_s$ (emu g <sup>-1</sup> )	2.574	2.271	1.615
$M_r$ (emu g <sup>-1</sup> )	0.080	0.169	0.084
$H_c$ (Oe)	35.7	97.8	99.1

All samples exhibit narrow hysteresis loops with weak ferromagnetic behavior, which could also be a result of disordered surface spins [19], showing a decrease of the saturation magnetization ( $M_s$ ) with increasing particle size, the result of which are all in agreement with the earlier reports [23]. As seen in Fig. 3, the remanence magnetization ( $M_r$ ) value increases at first and then drops. The remanence maximum is centered around 37.07 nm for a sample calcined at 800 °C. Further increase in crystallite size above 37.07 nm lowers the remanence magnetization. A similar trend in ( $M_s$ ) is also observed in the case of Ni–Zn and Mn–Zn ferrites studies by Gh.R. Amiri et al [24]. The coercivity ( $H_c$ ) depends mainly on particle size and crystalline anisotropy constant [25]. The coercivity shows an increasing trend as the calcination temperature increases,

this can be attributed to the increase in particle size with the calcination temperature. C. Sujatha et al [18] observations account for the similar trend behavior.

#### 4. Conclusions

In summary, MgFeCrO<sub>4</sub> ferrite nanoparticles were successfully synthesized by using a sol-gel auto-combustion method. Later, the effects of calcination temperature on the structural and magnetic properties were studied using five characterization techniques, including XRD, FE-SEM, EDS, TGA and VSM respectively. The X-ray diffraction analysis confirmed the formation of single phase cubic spinel structure and when the calcination temperature was elevated, the diffraction peaks became sharper and narrower. FE-SEM studies revealed some agglomerated of spherical nanoparticles shape with fine size.

The chemical composition of the MgFeCrO<sub>4</sub> nanoparticles was performed by energy dispersive spectrum (EDS), demonstrating that the MgFeCrO<sub>4</sub> nanoparticles contained the elements of Mg, Fe, Cr, and O. The TGA analysis showed the completion of decomposition of the precursors at 700 °C calcination temperature. The VSM results indicate that the magnetic properties are dependent on the calcination temperature, and with the increase in the calcination temperature, the saturation magnetization decreases, while coercivity increases. The value of remanence magnetization increases at calcination temperature 700 to 800 °C and then drops at 900 °C. It can be observed that the structural and magnetic properties of MgFeCrO<sub>4</sub> ferrite nanoparticles change as a result of the increase in the calcination temperature, due to the rearrangements of divalent metal cations at different tetrahedral (A) and octahedral [B] sites.

#### References

- [1]H. Kiswanto, A. Puspitasari, E. Suharyadi, T. Kato, S. Iwata, IOP Conference Series: Materials Science and Engineering **367**, 012001 (2018).
- [2]A. Shinde, International Journal of Innovative Technology and Exploring Engineering **3**(4), 64 (2013).
- [3] M. Atif, M. Asghar, M. Nadeem, W. Khalid, Z. Ali, S. Badshah, Journal of Physics and Chemistry of Solids **123**, 36 (2018).
- [4]R. Kaur, A. Hasan, N. Iqbal, S. Alam, M. K. Saini, S. K. Raza, Journal of Separation Science **37**(14), 1805 (2014).
- [5]A. E .Gash, T. M. Tillotson, J. H. Satcher Jr, J. F. Poco, L. W. Hrubesh, R. L. Simpson, Chemistry of Materials **13**(3), 999 (2001).
- [6]M. Margabandhu, A. Sendhilnathan, S. Senthilkumar, D. Gajalakshmi, Brazilian Archives of Biology and Technology **59**(SPE2), (2016).
- [7]Y. Qu, H. Yang, N. Yang, Y. Fan, H. Zhu, G. Zou, Materials Letters **60**, 29-30), 3548 (2006).
- [8]A. M. Mohammad, S. M. A. Ridha, T. H. Mubarak, International Journal of Applied Engineering Research **13**(8), 6026 (2018).
- [9]A. Mohammad, S. Aliridha, T. Mubarak, Digest Journal of Nanomaterials & Biostructures (DJNB) **13**(3), (2018).
- [10]Z. T. Khodair, A. A. Kamil, Y. K. Abdalaah, Physica B: Condensed Matter **503**, 55 (2016).
- [11]K. Ramarao, B. R. Babu, B. K. Babu, V. Veeraiah, S. Ramarao, K. Rajasekhar, A. V. Rao, Physica B: Condensed Matter **528**, 18 (2018).
- [12]N. Rezlescu, E. Rezlescu, C. Pasnicu, M .Craus, Journal of Physics: Condensed Matter **6**(29), 5707 (1994).
- [13]X.-D. Zhou, W. Huebner, Applied Physics Letters **79**(21), 3512 (2001).
- [14]R. Panda, R. Muduli, G. Jayarao, D. Sanyal, D. Behera, Journal of Alloys and Compounds **6**(69), 19 (2016).
- [15]M. Lakshmi, K. V. Kumar, K. Thyagarajan, Advances in Nanoparticles **5**(01), 103 (2016).

- [16]M. Azim, M. Chaudhry, N. Amin, M. Arshad, M. Islam, S. Nosheen, M. Ahmad, H. Anwar, M. Waseem, G. Mustafa, *Digest Journal of Nanomaterials and Biostructures* **11**(3), 953 (2016).
- [17]S. Gowreesan, A. R. Kumar, *Journal of Materials Science: Materials in Electronics* **28**(6), 4553 (2017).
- [18]C. Sujatha, K. V. Reddy, K. S. Babu, A. R. Reddy, K. Rao, *Ceramics International* **38**(7), 5813 (2012).
- [19]Y. Qiu, Y. Luo, Z. Zou, Z. Tian, S. Yuan, Y. Xi, L. Huang, *Journal of Materials Science: Materials in Electronics* **25**(2), 760 (2014).
- [20]D. Mane, D. Birajdar, S. Patil, S. E. Shirsath, R. Kadam, *Journal of Sol-Gel Science and Technology* **58**(1), 70 (2011).
- [21]S. Nag, A. Roychowdhury, D. Das, S. Das, S. Mukherjee, *Journal of Magnetism and Magnetic Materials* **466**, 172 (2018).
- [22]P. Aghav, V. N. Dhage, M. L. Mane, D. Shengule, R. Dorik, K. Jadhav, *Physica B: Condensed Matter* **406**(23), 4350 (2011).
- [23]S. Phokha, S. Pinitsoontorn, S. Rujirawat, S. Maensiri, *Physica B: Condensed Matter* **476**, 55 (2015).
- [24]G. R. Amiri, M. Yousefi, M. Abolhassani, S. Manouchehri, M. Keshavarz, S. Fatahian, *Journal of Magnetism and Magnetic Materials* **323**(6), 730 (2011).
- [25]A. Ashrafizadeh, A. Ghasemi, A. Paesano Jr, C. F. C. Machado, X. Liu, A. Morisako, *Journal of Alloys and Compounds* **506**(1), 279 (2010).